THESIS FOR THE DEGREE OF LICENTIATE OF ENGINEERING

Corrosion of AlMg3.5 alloy from Studsvik R2 reactor under simulated cementitious repository conditions

Marvin Schobel

Department of Chemistry and Chemical Engineering

CHALMERS UNIVERSITY OF TECHNOLOGY

Gothenburg, Sweden 2025

Corrosion of AlMg3.5 alloy from Studsvik R2 reactor under simulated cementitious repository conditions

Marvin Schobel

Technical report no 2025:10

Department of Chemistry and Chemical Engineering

Chalmers University of Technology

SE-412 96 Gothenburg

Sweden

Telephone +46 (0)31-772 1000

Cover: Schematic illustration of process from reactor to graph of corrosion rate, including reactor vessel, samples, and setups.

Chalmers digitaltryck

Gothenburg, Sweden 2025

Corrosion of AlMg3.5 alloy from Studsvik R2 reactor under simulated cementitious repository conditions

Marvin Schobel

Nuclear Chemistry

Department of Chemistry and Chemical Engineering

Chalmers University of Technology

Abstract

Decommissioning nuclear research reactors produces low- and intermediate-level radioactive waste which has to be confined for extended time scales. The current repository concept is predicated on encapsulation in concrete. The alkaline conditions of the cement pore water with pH values up to 14 in early stages can be advantageous for certain radionuclides due to their precipitation. However, for other materials, including reactive corrosive metals such as aluminum, it can foster their corrosion. The decommissioned Studsvik R2 research reactor contained an AlMg3.5 alloy for core internals and the reactor tank. Acute aluminum corrosion is known to be fast at high pH and then slow down due to the formation of a protective oxidation layer. The initial corrosion produces significant amounts of hydrogen which can lead to pressure build up when encapsulated in concrete. This pressure increase can produce cracks which can be migration pathways for radionuclides. The corrosion rates of the Studsvik R2 reactor alloy have been studied while exposing it to concrete with elevated water/cement ratios of 0.7 (ca. 0.45 in commercial concrete). An artificial simplified weathered cement water was used to examine its suitability to assess long-term corrosion rates in concrete. Corrosion rates were determined by hydrogen-induced pressure measurements in overpressure bottles and stainless-steel pressure vessels, as well as by mass loss evaluation. The initial corrosion rates were high with more than 10^4 µm/y and then slowed down to values in order of 10^2 µm/y after 2000 hours of exposure in concrete. In pressure vessels, a delayed increase of the corrosion rates in cement water was found which is assumed to be caused by the surface coverage of hydrogen bubbles. Future and ongoing studies will contain different lower pH and climate friendly concrete compositions, pre-treatment of the alloy and the examination of other reactive metals that are relevant for Swedish repositories.

Keywords: Hydrogen, Radioactive-waste, Repository, Corrosion, Aluminum, AlMg3.5, Cement, Concrete, Fly Ash

List of Publications

Paper I (peer-reviewed conference paper)

M. Schobel, C. Ekberg, T. Retegan Vollmer, and A. Puranen, “Corrosion Characteristics of Studsvik R2 Al-Alloy by Hydrogen Evolution Under Simulated Repository Conditions,” in WM2025 Conference, Phoenix, Arizona, USA, 2025.

Contributions: Conceptualization, M.S. and A.P.; methodology, M.S. and A.P.; software, M.S..; validation, M.S. and A.P.; formal analysis, M.S.; investigation, M.S.; resources, M.S.; data curation, M.S.; writing—original draft preparation, M.S.; writing—review and editing, A.P., T.R.V., C.E.; visualization, M.S.; supervision, A.P.; project administration, A.P.; funding acquisition, A.P.

Paper II (published)

M. Schobel, C. Ekberg, T. Retegan Vollmer, F. Wennerlund, S. Hedström, and A. Puranen, “Study of Corrosion Characteristics of AlMg3.5 Alloy by Hydrogen-Induced Pressure and Mass Loss Evaluation Under Simulated Cementitious Repository Conditions,” Corrosion and Materials Degradation, vol. 6, no. 3, pp. 27, 2025.

Contributions: Conceptualization, M.S. and A.P.; methodology, M.S. and A.P.; software, M.S. and F.W.; validation, M.S. and A.P.; formal analysis, M.S.; investigation, M.S.; resources, M.S.; data curation, M.S.; writing—original draft preparation, M.S.; writing—review and editing, A.P., T.R.V., C.E., S.H.; visualization, M.S.; supervision, A.P.; project administration, A.P.; funding acquisition, A.P. and S.H.

List of Abbreviations

MTR	Material Testing Reactor
BOCA	Boiling Capsules
BWR	Boiling Water Reactor
PWR	Pressurized Water Reactor
MQ	Milli-Q® (Ultrapure Water)
CW	Cement Water
BET	Brunauer, Emmett and Teller
XRF	X-ray Fluorescence
XRD	X-ray Diffraction
SEM	Scanning Electron Microscope

Contents

1. Introduction

The decommissioning and dismantling of nuclear research reactors produces low- and intermediate-level radioactive waste. Proper disposal in repositories for extended timespans and withstanding natural degradation as well as waste-induced alteration processes has to be conducted for reasons concerning the environment and public safety [1, 2]. Low- and intermediate-level radioactive waste, in Sweden, is typically encapsulated in concrete before being stored in drums [3] or concrete boxes. The encapsulation of the decommissioning waste serves as a barrier of radiation, and sorption and therefore promotes radionuclide retention in long-term [3-5]. Encapsulation in concrete, however, also comes with pH in the pore water up to 14 in the early stages and eventually decreases to 10 or lower [1, 4, 6]. This can be advantageous for some heavy-element radionuclides because it allows their precipitation as hydroxides but promotes the corrosion of some metals such as aluminum [1, 4, 6].

Relatively little research has been done on aluminum corrosion under simulated repository conditions, and no research has been done on the Studsvik R2 alloy prior to this work. Available studies on aluminum metal under alkaline or simulated repository conditions have reported initial corrosion rates in the range of 10^3 µm/y after 2 weeks to 20 days, which then rapidly decreased due to the formation of the protective oxidation layer, reaching rates in the range of 10^2 µm/y within 26 to 80 days [1, 6-8]. While previous studies mainly focused on electrochemical methods [9, 10] and mass loss evaluation [1, 6, 11] to assess certain corrosion characteristics of the aluminum, this study focusses on hydrogen gas-induced pressure measurements, supported by evaluation of mass loss. The magnesium content of the R2 alloy is less than 7%. Therefore, stress corrosion cracking of the material does not have to be taken into account [12]. The contained magnesium, however, might contribute to the formation of hydrogen gas, which is a known product of its corrosion [13-17]. Yet, the small percentage of magnesium in the alloy suggests only a minor contribution to this. In this study, corrosion characteristics of the Studsvik R2 AlMg3.5 alloy has been examined for the first time under repository conditions, simulating the conditions of Swedish repositories for low- and intermediate-level radioactive waste to evaluate if measures have to be taken before disposal of the material. This has been done using two different setups and three different methods.

Moreover, different kinds of concrete compositions were tested to consider more climate friendly waste-conditioning material, while also lowering the pH.

2. Background

2.1 Studsvik R2 Reactor, Sweden

Sweden's first nuclear power reactor in Ågesta was in operation mainly for district heating in the south Stockholm area between 1964 and 1974. The oldest research reactor, R1, is located at the Royal institute of technology and was in operation between 1954 and 1970. Two more research reactors were located in Studsvik, R2 and R2-0, and were critical between 1960 and 2005. Studsvik has been the national center for nuclear research activities since 1960. Today, the site offers laboratories for irradiated nuclear fuel and materials testing as well as facilities for waste treatment and storage [3].

The R2 tank-in-pool reactor in Studsvik (Sweden) was in operation since 1960 [18]. Reactors of the same type, designed by Allis-Chalmers (USA), were also built in South Africa (Safari), Netherlands (Petten) and USA (Oak Ridge) of which the first two are still operating. It contained an Al-alloy vessel at one end of a large Al-liner open pool with sections that served as storage for spent fuel. While in commercial power reactors, it is not possible to run fuel experiments up and beyond failure, it was possible in the Studsvik R2 testing reactor. It was used as a testing facility for water reactor fuel and for high temperature gas cooled reactor fuel. Initially, a high-enriched uraniumsilicide fuel was used (>90 % U-235) which was later converted to high assay low-enriched uranium fuel (<20 % U-235). The reactor core in the R2 irradiation facilities had a 8×10 lattice where the outer rows were filled with beryllium reflector pieces [19]. The core consisted of 46 fuel elements of material testing reactor (MTR) plate type with beryllium reflector assemblies, in-pile loops, irradiation rigs and aluminum fillers [18, 19]. The core contained six control rods; each fuel element contained 250 g of ^{235}U [18]. 20 different positions were possible for experiments. Moreover, the possibility to adapt to different experimental programs existed [18, 19]. As core coolant and moderator, light water was used. In 1968, the reactor power was set to 50 MW(th) [20]. The reactor was re-built during 1984 and 1985 with a new vessel [19].

Base irradiation of tests fuels was conducted in boiling capsules (BOCA rigs) while some base irradiations and all irradiations under power changes (ramp tests) with ^{3}He as a neutron absorber were performed in an in-pile loop simulating boiling water reactor (BWR) or pressurized boiling reactor (PWR) conditions. The length of the active fuel was 0.6 m. A second reactor (swimming pool reactor) that could be moved to various irradiation positions known as R2-0 was operated at up to 1 MW(th) [19]. The facility also included beam tubes for neutron research including heavy water (D_2O) boxes for improved neutron thermalization [3].

The radioisotope production of the R2 reactor was limited by the operational cycle limits; the maximal neutron flux was 4×10^{14} n/cm^{2}s [19]. The isotopes could be produced in a large variety of conditions and positions in and around the R2 reactor vessel [18-20]. Isotopes that were being produced were e.g., ^{192}Ir for industrial gamma radiography, ^{153}Gd for bone scanning, ^{32}P and ^{35}S for biological research and ^{85}Sr, ^{89}Sr, ^{86}Rb, ^{153}Cd, ^{110}Ag, ^{59}Cr, ^{59}Fe, ^{45}Cs, ^{47}Cs, ^{90}Y, ^{186}Re and ^{63}Ni for medical research purposes [19]. After the reactor was re-built, there were two sets of irradiated R2 reactor tanks along with ancillary core compositions.

2.2 Nuclear waste disposal in Sweden

Operational waste from nuclear facilities in Sweden is usually classified as short-lived low- and intermediate-level waste. This is being disposed of in the repository for low- and intermediate-level short-lived waste (SFR) in Forsmark that was commissioned in 1988. Very low-level waste can also be disposed of in shallow land burials. Long-lived low- and intermediate-level waste is commonly stored at nuclear power plants, or at authorized facilities such as the Studsvik Tech Park. These waste materials are planned to be disposed in a future geological repository, SFL [3]. Spent fuel is stored at the central interim storage facility Clab in Oskarshamn pending encapsulation and disposal in the future spent fuel repository in Forsmark that was approved for construction in 2024.

2.3 Decommissioning of Studsvik R2 and R2-0

The decommissioning of the research reactors on the Studsvik site was conducted in three phases. Prior to final disposal, solid and liquid waste was stored on-site. The first phase included decontamination of the in-pile loops and dismantling of the reactors in the reactor pool. The second phase contained the dismantling of parts of pool structures and systems with high activity. The third phase was the main decommissioning phase, consisting of dismantling of all systems in the facility (primary, secondary, and auxiliary systems), decontamination of buildings and clearance measurements of buildings and materials. [21].

Different kinds of solid radioactive waste had to be disposed of. That included scrap metal that did not need any special treatment after demolition and scrap metal for melting in the Cyclife facility (Studsvik, Sweden). Three types of low-level radioactive waste had to be considered, including low-level combustible secondary waste, low-level waste from contaminated systems and low-level waste from decommissioning of building constructions. The decommissioning also produced activated reactor component waste [21]. In total, the decommissioning of the R2 reactor resulted in approximately 20 tons of aluminum alloy waste with varying radionuclide content. The aluminum alloy core components add up to about 5000 kg with the major radionuclides produced by activation being ^{3}H, ^{55}Fe, ^{59}Ni-, ^{60}Co and ^{63}Ni. The total activity of the core aluminum alloy components was about 13 TBq (reference date 2014-01-01) with most of the activity coming from ^{60}Co. The aluminum components contain a minor fraction of the total activity while other components such as irradiated stainless steel items dominate the total activity [22].

2.4 Corrosion of aluminum alloy

The commonly used aluminum alloys in nuclear research reactors are known to undergo an accelerated initial corrosion in alkaline environments which gradually slows down due to the formation of a protective oxidation layer within seconds to weeks, depending on the materials surface characteristics [1, 6]. Primary solid corrosion products, forming the oxide layer, are the amorphous Al_2O_3, followed by the formation of an metastable Al(OOH) and furthermore

$Al(OH)_3$ (Eq. 1-3) [1, 6-9, 23]. A Pourbaix diagram of aluminum is shown in Figure 1. The main driver of the eventual dissolution of the oxide layer under high pH conditions is believed to be the $[Al(OH)_4]^-$ ion (Eq. 4) which also works as the main phase of the aluminum corrosion product under repository conditions [23]. Metallic aluminum is only stable at highly reducing conditions. This is also clear from Figure 1.

However, the formation of the $[Al(OH)_4]^-$ ion is limited due to the solubility of the oxide and hydroxide phase [24-27]. The corrosion produces relatively large amounts of hydrogen which may lead to the formation of cracks in the concrete that can serve as pathways for radionuclides to migrate and, therefore, may disturb the long-term safety of repositories [1, 2, 4, 6-8, 10, 28]. The corrosion process is not impacted by oxygen availability [29]. The Studsvik R2 alloy from the reactor vessel is an AlMg3.5 alloy with a composition close to the commercial Al5154 alloy. Minor elements at approximately 0.1 to 0.3% concentration include Cr, Fe, Ti and Si.

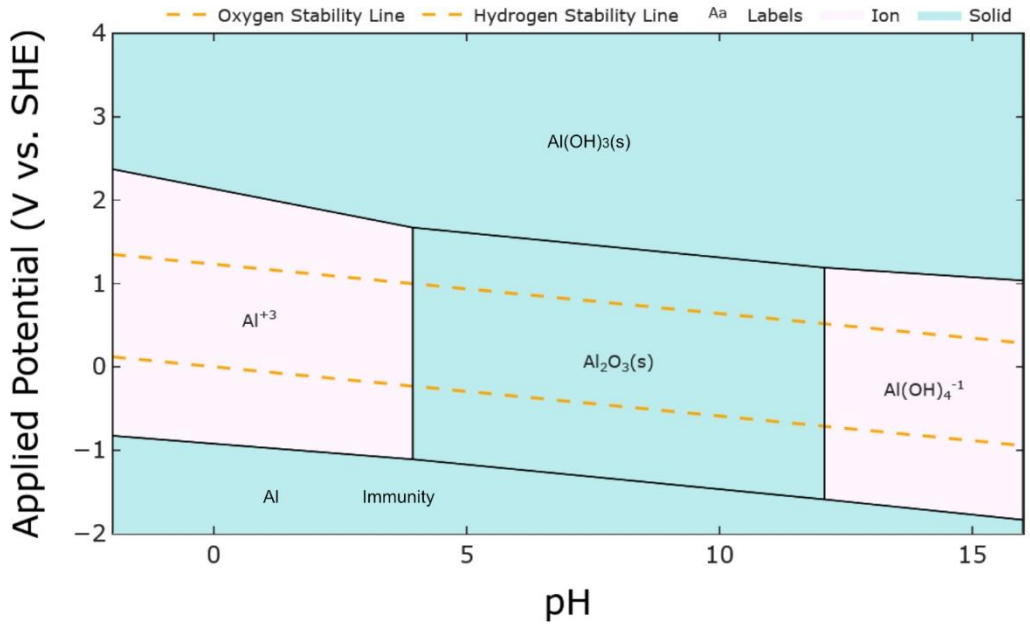

Figure 1: Pourbaix diagram of aluminum with a concentration of 10^{-3} mol, pH ranging from 0 - 16 and potential from -2 to 4. Ions are shown in grey, solid products in green. Dashed lines show the oxygen stability (top) and hydrogen stability lines [30-33].

$$2Al + 3H_2O \rightarrow Al_2O_3 + 3H_2 \qquad (Eq.1)$$

$$2Al + 4H_2O \rightarrow 2AlOOH + 3H_2 \qquad (Eq.2)$$

$$2Al + 6H_2O \rightarrow 2Al(OH)_3 + 3H_2 \qquad (Eq.3)$$

$$2Al + 2OH^- + 6H_2O \rightarrow 2Al(OH)_4^- + 3H_2 \qquad (Eq.4)$$

2.5 Alternative concrete compositions

2.5.1 Magnesium-based concrete

Alternative cement compositions have to be considered due to climate aspects, but also due to the high pH in standard Portland cement and the resulting rapid corrosion of aluminum [1, 4, 6]. Sorel cements, such as magnesium-oxysulfate cements, are known to have a higher resistance against environment-induced alterations and weathering while also having a lower pH compared to Portland cement. These materials are produced by magnesia, magnesium-oxysulfate and water by forming $Mg(OH)_2$ which becomes, in combination with magnesia and magnesium-oxysulfate, a very hard material comparable to regular cement. However, the production is complicated due to the limited solubility of $MgSO_4 \times 7H_2O$ at room temperature [34-36].

Another alternative of interest for Swedish repositories is magnesium-phosphate cement. It has a high early strength and is fast setting while also conferring a lower pH than regular Portland cement. It is prepared with a soluble acid phosphate which could commonly be KH_2PO_4 that forms the hard mineral struvite ($KMgPO_4 \times 6H_2O$) [34, 36-39].

2.5.2 Fly ash

The partial replacement of Portland cement by fly ash is employed to produce more climate friendly concrete since it decreases the amount of required Portland cement which causes the main CO_2 emissions in concrete and, moreover, fly ash is a waste product which can be

recycled that way [40]. The addition of fly ash reduces the compressive strength of the concrete, however, leads to the decrease of alkali carbonate reactions which are known to be the main reason for expansion cracking [40, 41]. It was also observed that carbonation in fly ash containing concretes is decreased which leads, next to the decrease in K^+ and Na^+ through less alkali carbonate reactions, to a decreased pH and should therefore slow down the corrosion of aluminum [40-43]. Ren et al. [41] observed a significant lower pH of 12.25 in concrete with 30 % fly ash replacement after only 21 days of curing time.

3. Materials & Methods

3.1 R2 alloy and aluminum metal

3.1.1 Sample preparation

Samples with 15 mm length and 5 mm diameter were machined from an unirradiated reference batch of the same material as the Studsvik R2 reactor vessel alloy. As reference, same-dimensioned samples were cut from 99.95 % purity aluminum (Thermo Scientific Chemicals, USA). For rate estimations, the geometric surface area was used since no exact surface area can be stated due to its corrosion-induced evolution.

3.2 Portland cement concrete and simplified artificial cement water

To prepare 250 g of concrete, 65.8 g of standard CEM I Portland cement (Chalmers Building Materials Lab, Sweden), 13.2 g of calcium carbonate (Limus 40, Nordkalk, Sweden), 132 g of standard sand (EN 196-1, Germany) and 46.1 ml ultrapure water (MQ) were mixed. The water-cement ratio was 0.7, which is higher than in conventional concrete to guarantee a continuous corrosion throughout the whole experiment without depleting the pore water content.

The artificial simplified cement water was prepared in a very simplified manner by dissolving 0.74 g NaCl as background electrolytes in 200 ml MQ water (10 mM NaCl). To adjust the pH and keep it constant at 12.4, about 0.43 g of CaO were added to Eppendorf tubes with perforated lid as shown in Figure 2. It was added to every solution-based experiment, the constant water circulation between sample tube and Eppendorf tube led to the adjustment of pH which was confirmed with a pH paper. The pH is lower than in fresh cement (pH > 13), aiming to mimic weathered cement water and represent longer term repository conditions.

3.3 Pressure bottle setup

All experiments were conducted in triplicates in an inert nitrogen-filled glovebox (<0.1 ppm O_2) to prevent aeration or hydrogen combustion and to simulate long-term repository conditions. 5 ml of concrete was filled into a 30 ml vial and the cleaned metal samples were immersed centrally in the concrete. After waiting for about 3-5 minutes until the viscosity of the concrete decreased, the vials were filled up to 20 ml with concrete. The sample vial was then quickly transferred to a 500 ml GL45 overpressure bottle (pressure plus+, DURAN Group GmbH, Germany), as seen in Figure 2, alongside a modified pressure, temperature and humidity sensor (T1, Aqara, China). The sensor was dismantled, and a bigger battery pack was attached as shown in Figure 3. It was coated with varnish to protect from humidity. The sensor was connected to a Raspberry Pi single board computer (Zero WH v.1.1, Raspberry Pi Ltd., UK) that was setup with a Zigbee-based broker and a Zigbee coordinator (CC2652R, Slaesh GmbH, Germany). To automatically collect the data from the sensor, a Python script was used. Changes in pressure, humidity and temperature triggered the sensor to wirelessly collect data. The overpressure bottles can withstand an overpressure of up to 1.5 bar. The sample size was chosen so that the pressure, considering complete corrosion of the sample, could not exceed this pressure. The bottles were sealed with bromobutyl septa (DURAN group GmbH, Germany) inserted in the lid to seal tightly and give the opportunity for liquid and/or gas samples. The same experimental setup was carried out with aluminum metal as reference.

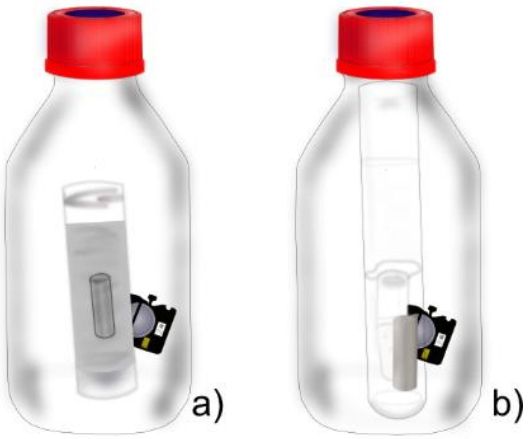

Figure 2: Pressure bottle setup. a) R2 alloy immersed in concrete and inserted in overpressure bottle alongside pressure sensor. b) R2 alloy immersed in CW and inserted in overpressure bottle. Both sealed with bromobutyl septa in lids [7].

Figure 3: Pressure, humidity and temperature sensor board with attached battery pack [7].

3.4 Pressure vessel setup

The samples were immersed in 20 ml of concrete using the same process as for the pressure bottle experiments. The sample tubes were inserted in 165 ml pressure vessels (Precision Fabrication LLC, USA) as seen in Figure 4. The pressure measurements were performed with a pressure gauge designed for hydrogen use (LEO-Record-H_2Ei, Keller, Switzerland). The size of the sample was chosen accordingly to the operating pressure of the vessels of 3447 kPa (test pressure 6895 kPa). Experiments were conducted at room temperature.

Figure 4: Pressure vessel setup for hydrogen pressure measurements [8].

3.5 Mass loss evaluation

Separate metal samples were placed in unpressurized plastic cups immersed in concrete and CW and exposed until undergoing destructive examination after months up to years of exposure. For destructive measurements, the containers were removed, and the concrete was cracked open. To remove concrete residues and the produced oxide, the samples were pickled for 20 minutes in 20 % nitric acid using an ultrasonic bath (Thermo Fisher Scientific, USA). Afterwards, they were soaked in silicon oil for approximately 24 hours to soften and loosen residues of the oxide layer. The layer was carefully scraped off and the pickling procedure was repeated. These steps were repeated until no mass loss was registered anymore. Full removal of the oxide was also confirmed with a portable microscope. Microscope pictures before (left) and after the removal of the oxide layer (right) are shown in Figure 5.

Figure 5: Corroded sample after 1 year exposure time (left) and sample after fully removing concrete residues and oxide (right) [8].

3.6 Alternative concrete compositions

3.6.1 Fly ash

Experiments were setup simultaneously to prior explained unpressurized plastic cups. However, the Portland cement was replaced to an extent of 30 % fly ash (Microsit M10 Hard coal, Backstein Engineering GmbH, Germany) for reduced pH. Moreover, this can be seen as

more climate friendly since fly ash is a waste product and can be recycled that way and Portland cement causes the highest CO_2 emissions in concrete production.

3.7 Calculation of corrosion rates

3.7.1 Pressure bottle setup

Corrosion rates were calculated by assuming Equations (1) - (4) with Al_2O_3 as an early amorphous corrosion product forming the passivating oxidation layer. $Al(OH)_3$ is the main solid product considering pH of solution and concrete [1, 6, 9, 23]. The pressure sensors recorded data with every change in pressure. Due to slight fluctuations in temperature and therefore also in measured pressure, averages of certain time spans were calculated to get an accurate estimation of the corrosion rates. Changes in pressure were used to calculate the amount of substance hydrogen and furthermore, the amount of substance of aluminum. Using the molar mass of aluminum, the mass could be calculated. Based on the mass, the corrosion rate was calculated in $g/m^2/y$. The surface area of the samples was not measured since it was too small to get accurate BET values. Moreover, the corrosion-induced evolution of the surface area was rather unpredictable and would change measured values throughout the experiment. The geometrical surface area was seen to be sufficient to calculate corrosion depth and therefore also the corrosion rates in µm/y. Uncertainties are given by differences between replicates and deviations between averaging time periods.

3.7.2 Pressure vessel setup

Corrosion rates of the pressure vessel setup were calculated as those of the pressure bottle setup. However, since this setup was less affected by temperature changes and measurement times could be controlled, the measured values have only been normalized to the average temperature and then used for further calculations. Uncertainties were calculated from replicates.

3.7.3 Mass loss evaluation

Corrosion rates from mass loss evaluations were calculated and extrapolated to µm/y using the specific mass loss and the geometric surface area.

3.8 Analytical methods

A portable XRF device (Niton XL5 Plus Thermo Scientific, USA) was used to measure the relative element concentration in the alloy and oxide. The measurements were conducted for samples in CW solution by temporary lifting them from the solution, rinsing them with MQ water and re-immersing them into the solution after measuring. Since this measurement started as an exploratory analysis, values for 4, 8 and 14 months of exposure were only measured in singles.

4. Results

4.1 Corrosion rates

During experiments in the pressure bottle setup, samples were immersed in concrete and CW. Immediately after immersing the samples in solutions, a strong coverage of hydrogen bubbles on the sample surface could be seen, as shown in Figure 6 (left). Experiments in concrete showed gas channeling after less than 1 month as seen in Figure 6 (right).

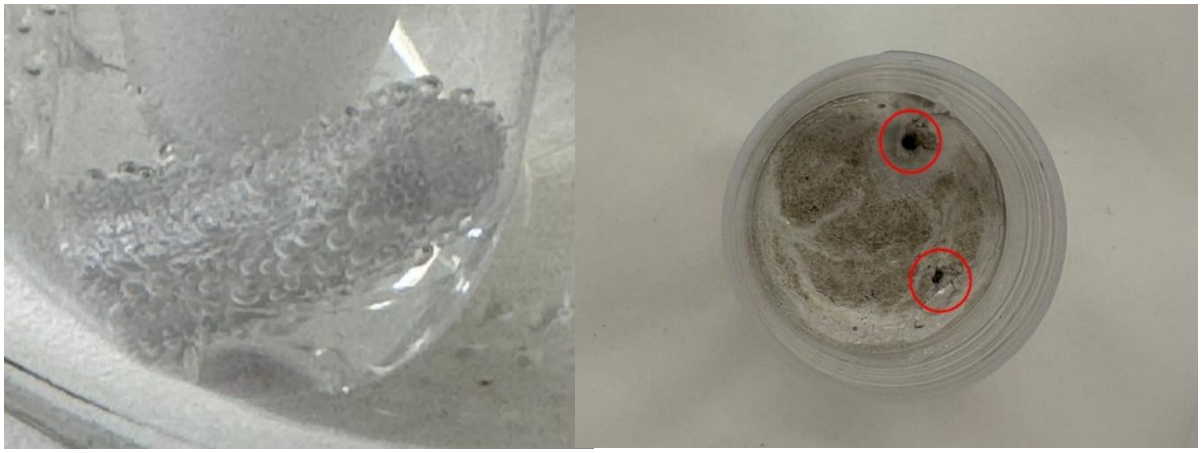

Figure 6: Formation of hydrogen bubbles of R2 alloy surface at immediate starting corrosion (left) [7]. Gas channels in sample immersed in concrete after 1 month exposure (right).

4.1.1 Pressure bottle setup

In data received from hydrogen-induced pressure measurements as shown in Figure 7, the rapid immediate corrosion was also seen with corrosion rates in the order of hundreds of thousands µm/y. They showed high uncertainties in the beginning which are most likely caused by slight time variations in sample preparation and the time-dependent average corrosion rates. The reaction rates dropped sharply after the first few hours and leveled off at a rate of 434 ± 178 µm/y after 4 weeks for the R2 alloy and to 606 ± 222 µm/y for the aluminum metal. Fitted rates suggest a trend of aluminum metal corroding faster than the R2 alloy.

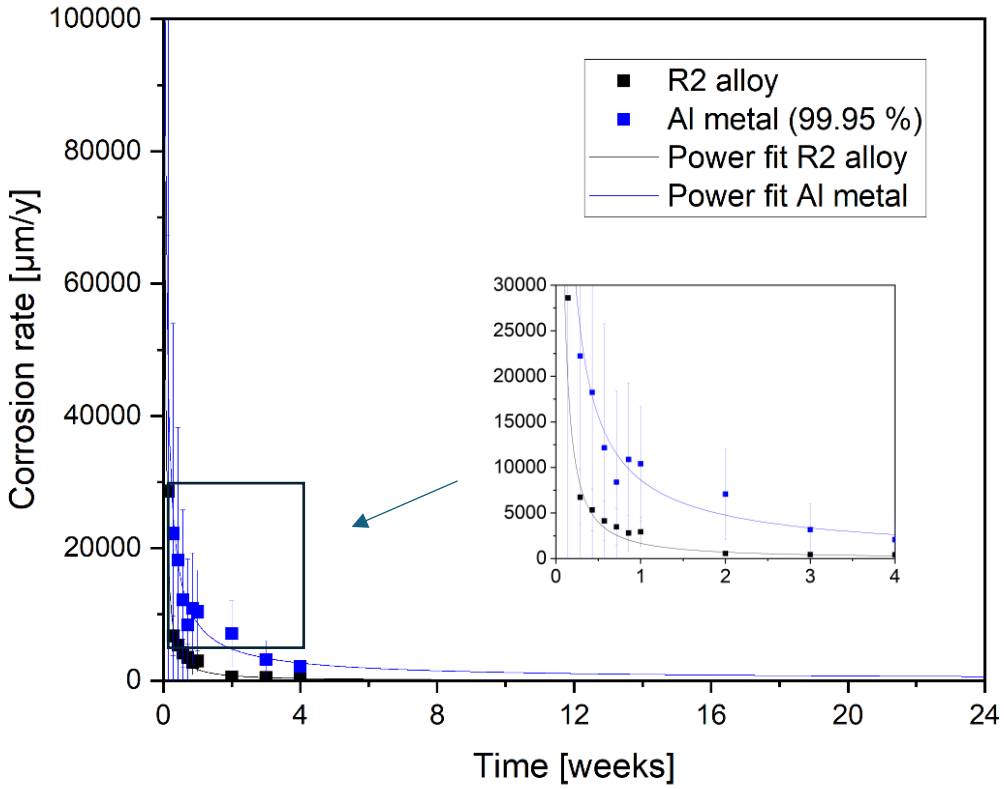

Figure 7: Corrosion rates in µm/y of R2 alloy and aluminum metal in concrete. Data extrapolated to 24 weeks. Cut out to lower corrosion rate and shorter time span [7]. Power fit of hydrogen pressure data according to [44].

The corrosion rates of the R2 alloy in artificial CW also showed extremely high initial values with high uncertainties as seen in Figure 8. Missing data between weeks 4 and 16 was caused by a change of the battery system. The R2 alloy showed corrosion rates of 397 ± 114 µm/y while the pure aluminum corroded faster at 458 ± 127 µm/y after 24 weeks. On long-term, the power fit also suggests that the aluminum metal corrodes slightly faster than the R2 alloy.

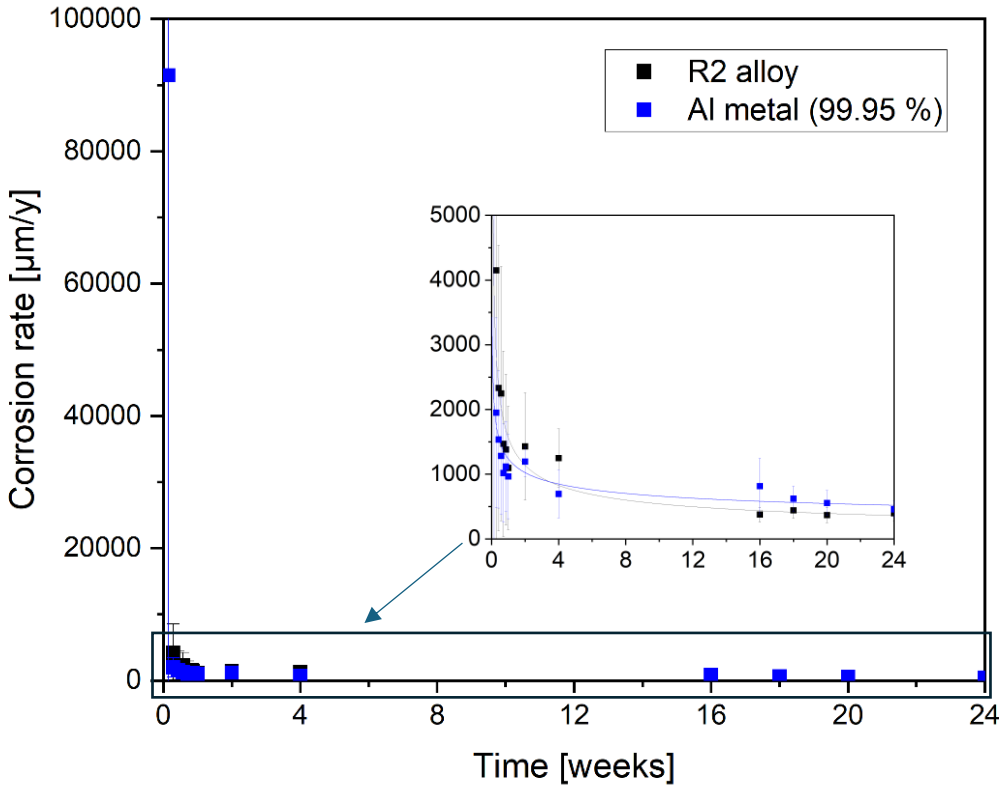

Figure 8: Corrosion rates in µm/y of R2 alloy and aluminum metal in CW. Data measured up to 24 weeks. Cutout to lower corrosion rate and shorter time span [7]. Power fit of hydrogen pressure data according to [44].

4.1.2 Pressure vessel setup

Corrosion rates in µm/y over a time span of 3300 hours of the R2 alloy in concrete measured by H_2-induced pressure and mass loss evaluation are shown in Figure 9. The rates were initially very high exceeding 10000 µm/y and then dropped significantly after a few days. After 2000 hours, the corrosion rate was below 500 µm/y and after 3300 hours it was 400 µm/y. Mass loss evaluation showed rates of 684 ± 73 µm/y after 1 month, 166 ± 34 µm/y after 6 months and 155 ± 26 µm/y after 1 year. A cutout is showing a logarithmic scale and a power fit to highlight the comparability of the results of the respective methods.

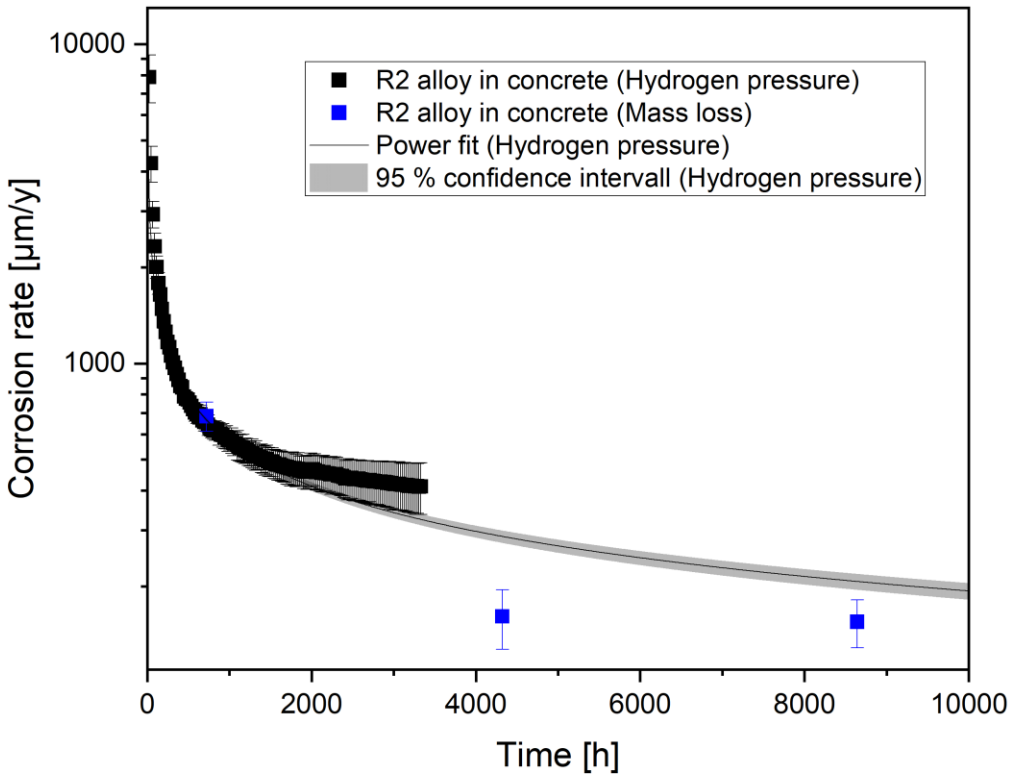

Figure 9: Corrosion rate of R2 alloy in concrete over a time period of 3300 hours calculated by H2-induced pressure (black). Uncertainties calculated from samples duplicates as standard deviation with Bessel's correction. Corrosion rate of R2 alloy in concrete calculated by mass loss evaluation (blue). Power fit of hydrogen pressure data with 95 % confidence interval according to [44] (continued data from [8]).

The corrosion rates in CW from gas-generation and mass-loss measurements are shown in Figure 10. A close-up view of rates calculated from gas evolution is seen in the inset. Initial corrosion rates were fluctuating and seemed to drop below 100 µm/y after a few hours. After approximately 100 hours, the rates start to increase again up to 800 µm/y after about 200 hours with decreasing uncertainties. Thereafter, corrosion rates decreased significantly to approximately 100 µm/y after 1700 hours and 65 µm/y after 3000 hours. Values from mass loss evaluation were at 55 ± 8 µm/y after 6 months and 3 ± 7 µm/y after 1 year which is in line with extrapolation of rates calculated from hydrogen gas evolution.

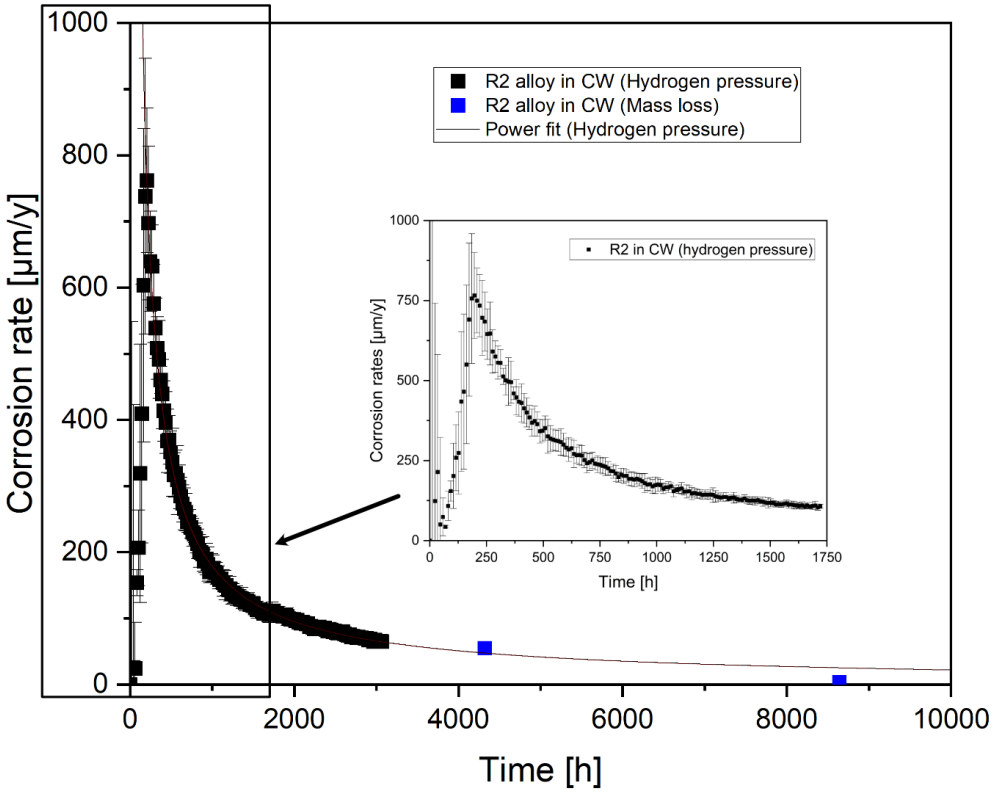

Figure 10: Corrosion rate of R2 alloy in CW over a time period of 3000 hours calculated by H2-induced pressure (black). Uncertainties calculated from sample duplicates with Bessel's correction. Cutout shows the rates detailed. Corrosion rate of R2 alloy in CW calculated by mass loss evaluation (blue). Power fit of hydrogen pressure data according to [44] (continued data from [8]).

The corrosion rates in CW were plotted against the corrosion rates in concrete in Figure 11 (left). The rates are compared over a time span of approximately 275 hours from 225 to 500 hours of exposure time. The uncertainties were calculated from the sample duplicates with Bessel's correction. The linear fit yields a coefficient of determination $R^2 = 0.98$ which suggests a linear correlation of the corrosion rate of the R2 alloy in both media. The corrosion rates of the R2 alloy in concrete (black) and CW (orange) over a time period of 250 hours is shown in Figure 11 (right). The rates are shown from 1250 hours to 1500 hours with linear fits to compare scale and decrease in corrosion rates in both media. The corrosion rate of the alloy in concrete is decreasing by 1.07 ± 5.95 µm/y. In CW, the rate is decreasing by 2.65 ± 1.72 µm/y. Considering uncertainties, no significant difference between slopes seems to be found.

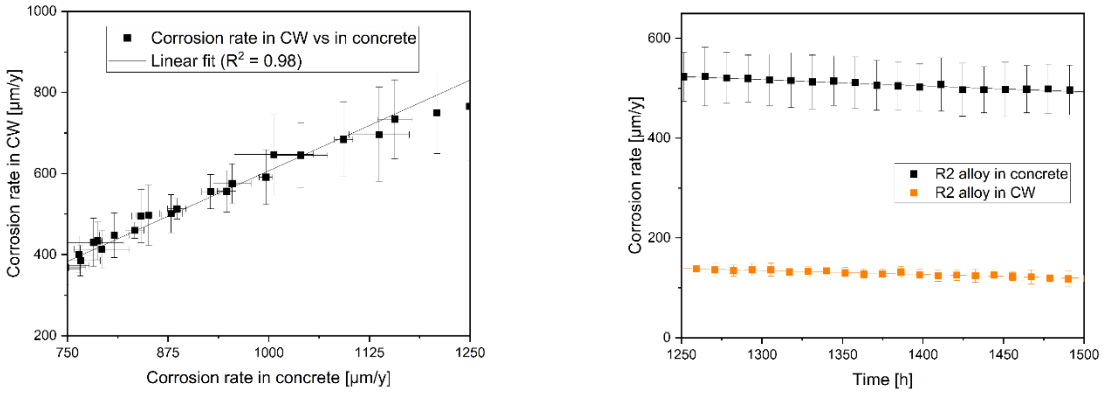

Figure 11: Corrosion rates in CW vs corrosion rates in concrete over a time span of ca. 275 hours from 225 to 500 hours of exposure time. Uncertainties calculated from sample duplicates. Fit with R^2 = 0.98 to highlight linear dependency of corrosion in both media (left) [8]. Corrosion rates of R2 alloy in concrete (black) and CW (orange) over a time span of 250 hours. Linear fits for both media to highlight similar decrease in corrosion rates (right).

4.2 Element analysis

Element analysis using XRF is shown in Table 2 as the relative concentration of aluminum, chromium, magnesium and iron of the samples before and after corrosion. Variations in concentrations can be caused by measuring different areas of the sample due to the changes in surface by corrosion. Aluminum concentration fluctuated slightly with no apparent trend. Chromium and iron also fluctuated slightly in very low magnitudes. Magnesium concentration decreased to values below the detection limit.

Table 1: Relative element concentration of Al, Cr, Mg and Fe of original sample, single samples after 4 and 8 months of exposure and triplicates after 12 months (LOD = Limit Of Detection). Uncertainties by device and repetitive measurements (continued data from [7]).

	Initial	4 months*	8 months *	14 months*
Element	%	%	%	%
Al	95.7 ± 0.13	92.3 ± 0.44	96.3 ± 0.20	93.1 ± 0.26
Cr	0.23 ± 0.00	2.04 ± 0.05	0.68 ± 0.01	0.48 ± 0.06
Mg	3.52 ± 0.13	1.57 ± 0.51	LOD <0.3	LOD <0.3
Fe	0.29 ± 0.01	1.55 ± 0.07	0.99 ± 0.03	1.36 ± 0.04

**repetitive measurements of single sample*

4.3 Alternative concrete compositions

4.3.1 Fly ash

The corrosion rate of the R2 alloy in ongoing experiments after 1 month exposure in concrete with Portland cement replaced 30 % by fly ash (CEM II/B-V) is shown in Figure 12. It is compared to the rates of R2 alloy in concrete with Portland cement without fly ash replacement and in CW. The rates were obtained from mass loss evaluation. It could be seen that corrosion rate of the R2 alloy in ordinary concrete was at 684 ± 73 µm/y after 1 month whereas with a 30 % fly ash replacement, it was at 179 ± 71 µm/y. Containing fly ash, the rate decreased to 66 ± 32 µm/y after 3 months. This value is slightly higher than the rate in ordinary concrete after 6 and 12 months.

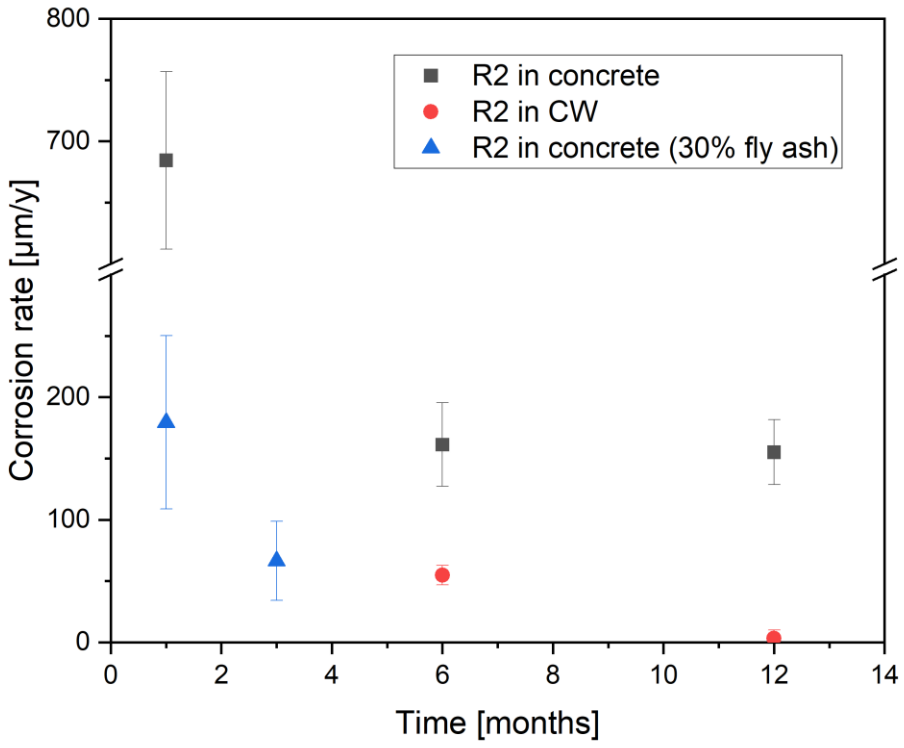

Figure 12: Corrosion rates of R2 alloy in ordinary concrete (black), with 30 % fly ash replacement (blue) and in CW (red) after 1, 3, 6 and 12 months discovered via mass loss evaluation. Uncertainties by standard deviation of triplicates.

5. Discussion

5.1 Hydrogen-induced pressure measurement

5.1.1 Pressure bottle setup

High corrosion rates with large uncertainties were measured in the beginning of the experiment. The large uncertainties were caused by various factors in the data analysis. The main factor impacting early corrosion rates was the immediate beginning of corrosion when immersing the sample into concrete or CW. Differences in preparation time, also impacted by working inside the glovebox, lead to differences in early corrosion rates between triplicates. Since the sensors sent data whenever a change of pressure, humidity or temperature was detected, and experiments were supposed to give long-term data, time span dependent averages of the corrosion rates were calculated. These averages could also lead to increased uncertainties. However, with the passing of time, the uncertainties leveled out and data on longer term was seen with smaller uncertainties. The extremely high corrosion rates in the beginning were consistent with unprotected surfaces and acute corrosion causing the formation of a protective oxide layer [1, 6-9]. The initial corrosion mainly produced Al_2O_3 incorporated in the oxide layer, while the long-term corrosion led to the incorporation of $Al(OH)_3$ in the layer [1, 6-9, 23].

A fast decrease in corrosion rates of both pure aluminum and R2 alloy in concrete, as well as in CW, was caused by the protection of the surface after the formation of an oxide layer [1, 6-8]. In both media, concrete and CW, the formation of hydrogen bubbles on the surface could also lead to a temporary protection of the surface and therefore slower corrosion rates as shown in Figure 6. However, this effect occurred stronger in CW. After a few weeks, the corrosion rates keep decreasing but at a much slower rate, shown by fitting the power law as suggested in literature [7, 44].

Long-term corrosion rates in concrete (shown in Figure 7) slowed down less rapidly compared to CW (shown in Figure 8) and long-term trends for the R2 alloy in concrete suggest slower

corrosion than for pure aluminum which was most likely caused by the 99.95 % purity of the latter and known rapid aluminum corrosion under alkaline conditions [1, 4, 6-8, 10, 28]. Other elements in the R2 alloy could inhibit corrosion. In CW, both materials showed similar corrosion rates.

5.1.2 Pressure vessel setup

The corrosion rates were measured during a time span of 2000 hours as shown in Figure 9. High corrosion rates of up to 10000 µm/y in concrete were consistent with the early formation of the oxide layer in acute corrosion [1, 6-9]. The corrosion rates in the pressure bottle setup were much higher, which can be explained through the faster preparation time of the sample. An initial fast, and with passing time, more constant decrease of the corrosion rates was also consistent with the pressure bottle setup and previous studies [1, 6, 7, 9]. The high initial corrosion rates in both setups were consistent with the early formation of gas-pressure-induced channels in the concrete as seen in Figure 6. These could become pathways for radionuclides [1, 2, 4, 6-8, 10, 28].

In CW, the higher time resolution of the pressure vessel and not calculating time dependent averages experiments showed a new trend that has not been seen before in the pressure bottle experiments. Before an increase to high corrosion rates of about 800 µm/y after 100 hours, a decrease with fluctuations and large uncertainties between the replicates was noticed as seen in Figure 10. Uncertainties could, again, be explained by differences in preparation time but the fluctuations were most likely caused by the surface coverage of the sample through the formation of hydrogen bubbles immediately after immersing the samples. The formation and release of the bubbles contributed to the uncertainties and latter to the delayed increase in corrosion rates after 100 hours. Another factor with could have a small impact in the delayed start of strong acute corrosion could be the diffusion of hydrogen in water [45]. After the delayed increase in corrosion rates, a decrease was discovered consistently with the protection of the surface through the oxide layer [1, 6-9, 23]. The corrosion rates in general, however, were lower than in concrete. This can be explained by the very simplified composition and lower pH of the cement water. The pH displays weathered cement water under granitic conditions and represents long-term repository conditions. The corrosion in both media was

plotted against each other in Figure 11 over a time period of 275 hours between 225 and 500 hours of exposure time. This yielded a linear function suggesting the linear correlation of the corrosion of the R2 alloy in both media which implies that the corrosion in CW can be used to assess corrosion rates in concrete to simplify the experimental procedure. The corrosion in both media between 1250 and 1500 hours was also plotted which showed a similar deceleration in decrease of the corrosion rates which supports the assumption.

Mass loss evaluations showed corrosion rates for R2 alloy in concrete of 684 µm/y after 1 month, 161 µm/y after 6 months and 155 µm/y after 1 year. The data from the pressure vessel experiments has been extrapolated with a power fit [7, 44] and is in CW within or in concrete close to the uncertainty range of these values. Considering the long-term extrapolation of the hydrogen-induced pressure measurements and the heteroscedasticity of the data, this suggests comparability of the results from both methods, however, has to be observed continuously.

5.2 Element analysis

While measuring the relative element concentration of the ongoing experiments, the oxide layer became too thick to measure the sample. Aluminum concentrations fluctuated between 92.3 ± 0.44 % and 96.3 ± 0.20 %. This could be caused by different accumulations of aluminum due to the uneven surface caused by corrosion. However, the aluminum concentration decreased at first from 95.7 ± 0.13 % to 92.3 ± 0.44 % after 4 months of exposure which could also be caused by the formation of the oxide layer [1, 6, 7, 9, 23]. The oxide layer might have been too thin, so that the actual alloy was measured. After 8 months, the concentration increased again to 96.3 % which is consistent with the formation and the thickening of the oxidation layer. After 14 months of exposure the concentration decreased to 93.1 ± 0.26 % which could be caused by the limited dissolution of $Al(OH)_3$ and Al_2O_3 at given alkaline conditions [8, 24-27].

The magnesium concentration decreased from its initial concentration of 3.52 ± 0.13 % to 1.57 ± 0.51 % after 4 months. After 8 and 14 months, no magnesium was detected by XRF. This could be related to the thickness of the oxidation layer and therefore the measurement of the layer and not the actual alloy, which is consistent with the previously described trend of

aluminum. That would imply that magnesium cannot be found in the oxidation layer which can be explained by the dissolution of magnesium and the evolving $Mg(OH)_2$ [13, 16].

5.3 Alternative concrete composition

Ongoing experiments in concrete with 30 % fly ash replacement of the cement showed much lower corrosion rates of the R2 alloy as seen in Figure 12. This can be explained by inhibited alkali carbonate reactions in the concrete, and therefore a decreased concentration of K^+ and Na^+, causing a decreased pH compared to regular Portland cement concrete [41]. The decreased compressive strength of this alternative concrete composition might be negligible considering a reduced expansion cracking through the decrease of alkali carbonate reactions [41]. Another factor for the decreased pH is the limited carbonation through partial cement replacement by fly ash [43].

6. Conclusion

The trend of mass loss examinations given by evaluation of the samples after 1, 6 and 14 months were consistent with the extrapolation from hydrogen-induced pressure analysis for the corrosion rates in both pressure bottles and gastight vessels. Differences between pressure bottles and pressure vessel experiments were caused by preparation time and less accuracy of bottle data. However, the pressure bottle setup gave reasonable and quick results with similar trends and can be used for further initial investigations. The higher accuracy of the pressure vessel experiments showed delayed corrosion due to the fast sample surface coverage by hydrogen bubbles in CW.

Despite high acute corrosion rates, they decrease rapidly to slow rates due to the formation of the protective oxide layer which is advantageous for long-term storage of the material. However, the evolution of gas channels after only 1 month of exposure visualized the very strong acute corrosion of the alloy. Considering this, ongoing experiments are carried out with samples including partial fly ash replacement of cement to reduce the pH (8-11) compared to standard Portland cement type I concrete (> 13) after curing. Acute corrosion rates of samples immersed into concrete containing 30 % of fly ash replacement showed significantly lower corrosion rates after 1 month.

7. Future outlook

Since the acute corrosion was very strong and led to cracking of concrete in early stages, further options should be evaluated. As it has already been started to pursue, different compositions of concrete with varying pH values, compressive strength and workability will be tested. To begin with, experiments with 10, 30 and 45 % replacement of the cement by fly ash are being carried out. Also, experiments with partial replacement of the cement by magnesium phosphate and/or magnesium oxysulfate will be conducted. Both of these alternative compositions are environmentally friendlier and have a lower pH which will be advantageous to prevent corrosion of aluminum. Another measure will be to pre-oxidize the material before encapsulating it in concrete. Moreover, surface analyzation with XRD and SEM are planned to evaluate the corrosion mechanisms.

Further studies will also be conducted with different materials that are relevant for Swedish repositories, such as Thorium metal. Continuing deconstructive measurements will be used as determination of oxide layer thickness by analysis of sample cross-sections with methods such as scanning electron microscopy.

More accurate estimations of long-term corrosion rates can be conducted by longer exposure times. These will also help to determine the suitability of experiments in cement water solutions for later tests on long-term corrosion characteristics.

For further studies, the pressure bottle setup will be used, along with the pressure vessels, to study corrosion characteristics for different materials. To improve the bottle setup, the sensor system was replaced by a temperature, humidity and pressure sensor (BME280, Bosch, Germany) on a sensor board (Seeed, China) and connected to a single board computer (ESP32-WROOM-32E, Espressif Systems, China) that sends data points for given time spans.

Acknowledgements

I want to express my gratitude to AB Svafo and the Swedish Nuclear Fuel and Waste Management Co (SKB) for funding this research.

Thank you to my supervisor Anders Puranen for his innovative ideas, guidance and for finding time for a lot of progress meetings and scientific discussions whenever it was needed. And not to forget, for a lot of fun times. Thank you to Christian Ekberg for the supervision at Chalmers and the help with administrative and scientific tasks to deal with. Thank you to Teodora Retegan Vollmer for her guidance, help, trust and for taking me to her dentist to measure my samples. Yes, I measured samples at a dentist. Thank you to Svante Hedström for his valuable comments and discussions. Thank you to Torbjörn Jönsson for machining my samples.

Thank you to my colleagues, not only for scientific advice, but also for making this journey a very fun one. Thanks to you, I spend a lot of my time laughing and enjoying my work which is not self-evident. I did not only have fun, but I also even made some very deep connections and had a lot of meaningful conversations. A special thank you to my office and my extended office for not only tolerating my craziness and regular freakouts, but also for embracing them and for always making me feel seen. Thanks to the opportunity to work here, I found a very special person on this journey, and I am very grateful for that.

And finally, thank you to my friends and family for always supporting me and my work even though they did not understand a thing. Especially to my mother. I promise I will call more often.

References

[1] G. Herting, and I. Odnevall, "Corrosion of Aluminium and Zinc in Concrete at Simulated Conditions of the Repository of Low Active Waste in Sweden," *Corrosion and Materials Degradation,* vol. 2, no. 2, pp. 150-163, 2021.

[2] L. P. Santana, "Management of radioactive waste: A review," *Proceedings of the International Academy of Ecology and Environmental Sciences,* vol. 6, no. 2, pp. 38, 2016.

[3] SSM, *Kingdom of Sweden - ARTEMIS. Self-assessment Report 2023*, The IAEA Integrated Review Service for Radioactive Waste and Spent Fuel Management, Decommissioning and Remediation (ARTEMIS), 2023.

[4] H. Kinoshita, P. Swift, C. Utton, B. Carro-Mateo, G. Marchand, N. Collier, and N. Milestone, "Corrosion of aluminium metal in OPC- and CAC-based cement matrices," *Cement and Concrete Research,* vol. 50, pp. 11-18, 2013.

[5] M. Atkins, and F. Glasser, "Application of Portland cement-based materials to radioactive waste immobilization," *Waste Management,* vol. 12, no. 2-3, pp. 105-131, 1992.

[6] M. Tabrizi, S. Lyon, G. Thompson, and J. Ferguson, "The long-term corrosion of aluminium in alkaline media," *Corrosion science,* vol. 32, no. 7, pp. 733-742, 1991.

[7] M. Schobel, C. Ekberg, T. Retegan Vollmer, and A. Puranen, "Corrosion Characteristics of Studsvik R2 Al-Alloy by Hydrogen Evolution Under Simulated Repository Conditions," in WM2025 Conference, Phoenix, Arizona, USA, 2025.

[8] M. Schobel, C. Ekberg, T. Retegan Vollmer, F. Wennerlund, S. Hedström, and A. Puranen, "Study of Corrosion Characteristics of AlMg3. 5 Alloy by Hydrogen-Induced Pressure and Mass Loss Evaluation Under Simulated Cementitious Repository Conditions," *Corrosion and Materials Degradation,* vol. 6, no. 3, pp. 27, 2025.

[9] H. Ezuber, A. El-Houd, and F. El-Shawesh, "A study on the corrosion behavior of aluminum alloys in seawater," *Materials & Design,* vol. 29, no. 4, pp. 801-805, 2008.

[10] S.-I. Pyun, and S.-M. Moon, "Corrosion mechanism of pure aluminium in aqueous alkaline solution," *Journal of Solid State Electrochemistry,* vol. 4, pp. 267-272, 2000.

[11] M. Husaini, B. Usman, and M. B. Ibrahim, "Evaluation of corrosion behaviour of aluminum in different environment," *Bayero Journal of Pure and Applied Sciences,* vol. 11, no. 1, pp. 88-92, 2018.

[12] R. H. Jones, J. S. Vetrano, and C. F. Windisch, “Stress Corrosion Cracking of Al-Mg and Mg-Al Alloys, December 2004,” *Corrosion,* vol. 60, no. 12, 2004.

[13] S. Thomas, N. V. Medhekar, G. S. Frankel, and N. Birbilis, “Corrosion mechanism and hydrogen evolution on Mg,” *Current Opinion in Solid State and Materials Science,* vol. 19, no. 2, pp. 85-94, 2015.

[14] A. D. King, N. Birbilis, and J. R. Scully, “Accurate electrochemical measurement of magnesium corrosion rates; a combined impedance, mass-loss and hydrogen collection study,” *Electrochimica Acta,* vol. 121, pp. 394-406, 2014.

[15] M. Curioni, “The behaviour of magnesium during free corrosion and potentiodynamic polarization investigated by real-time hydrogen measurement and optical imaging,” *Electrochimica Acta,* vol. 120, pp. 284-292, 2014.

[16] Y. Yang, F. Scenini, and M. Curioni, “A study on magnesium corrosion by real-time imaging and electrochemical methods: relationship between local processes and hydrogen evolution,” *Electrochimica Acta,* vol. 198, pp. 174-184, 2016.

[17] G. Song, A. Atrens, and D. StJohn, “An hydrogen evolution method for the estimation of the corrosion rate of magnesium alloys,” *Essential readings in magnesium technology*, pp. 565-572, 2016.

[18] S. Sandklef, and H. Tomani, *Irradiation facilities for LWR fuel testing in the Studsvik R2 reactor*, Aktiebolaget Atomenergi, 1973.

[19] M. Grounes, H. Tomani, C. Graeslund, H. Rundquist, and K. Skoeld, “Studsviks R2 reactor-Review of the capabilities at a multi-purpose research reactor,” 1996.

[20] J.-H. Karlsson, M. Moren, B. Jonsson, H. Tomani, and B.-G. Bergdahl, “Flow measurements by noise analysis of thermocouple signals from the BOCA experiment at the Studsvik R2 reactor,” *Progress in Nuclear Energy,* vol. 43, no. 1-4, pp. 289-296, 2003.

[21] SSM, *Decommissioning of the Nuclear Reactors R2 and R2-0 at Studsvik, Sweden – General Data as called for under Article 37 of the Euratom Treaty*, 2009.

[22] S. N. AB, *N-13/073 Studsvik R2 och R2-0 - Avveckling - Bestämning av neutroninducerad aktivitet.*, 2014.

[23] F. Xiao, R. Yang, and Z. Liu, “Active aluminum composites and their hydrogen generation via hydrolysis reaction: A review,” *International Journal of Hydrogen Energy,* vol. 47, no. 1, pp. 365-386, 2022.

[24] I. Boukerche, S. Djerad, L. Benmansour, L. Tifouti, and K. Saleh, “Degradability of aluminum in acidic and alkaline solutions,” *Corrosion Science,* vol. 78, pp. 343-352, 2014.

[25] S.-M. Moon, and S.-I. Pyun, “The corrosion of pure aluminium during cathodic polarization in aqueous solutions,” *Corrosion Science,* vol. 39, no. 2, pp. 399-408, 1997.

[26] K. Emregül, and A. A. Aksüt, “The behavior of aluminum in alkaline media,” *Corrosion science,* vol. 42, no. 12, pp. 2051-2067, 2000.

[27] J. Zhang, M. Klasky, and B. C. Letellier, “The aluminum chemistry and corrosion in alkaline solutions,” *Journal of Nuclear materials,* vol. 384, no. 2, pp. 175-189, 2009.

[28] D. Jana, and D. G. Tepke, "Corrosion of aluminum metal in concrete–a case study." pp. 33-65.

[29] P. Mauret, and P. Lacaze, “Water corrosion studies of AlMg (5154) and AlCuMg (2024) aluminium alloys by gas chromatography,” *Corrosion Science,* vol. 22, no. 4, pp. 321-329, 1982.

[30] A. Jain, S. P. Ong, G. Hautier, W. Chen, W. D. Richards, S. Dacek, S. Cholia, D. Gunter, D. Skinner, and G. Ceder, “Commentary: The Materials Project: A materials genome approach to accelerating materials innovation,” *APL materials,* vol. 1, no. 1, 2013.

[31] A. M. Patel, J. K. Nørskov, K. A. Persson, and J. H. Montoya, “Efficient Pourbaix diagrams of many-element compounds,” *Physical Chemistry Chemical Physics,* vol. 21, no. 45, pp. 25323-25327, 2019.

[32] A. K. Singh, L. Zhou, A. Shinde, S. K. Suram, J. H. Montoya, D. Winston, J. M. Gregoire, and K. A. Persson, “Electrochemical stability of metastable materials,” *Chemistry of Materials,* vol. 29, no. 23, pp. 10159-10167, 2017.

[33] K. A. Persson, B. Waldwick, P. Lazic, and G. Ceder, “Prediction of solid-aqueous equilibria: Scheme to combine first-principles calculations of solids with experimental aqueous states,” *Physical Review B—Condensed Matter and Materials Physics,* vol. 85, no. 23, pp. 235438, 2012.

[34] E. Bernard, H. Nguyen, S. Kawashima, B. Lothenbach, H. Manzano, J. Provis, A. Scott, C. Unluer, F. Winnefeld, and P. Kinnunen, “MgO-based cements–Current status and opportunities,” *RILEM Technical Letters,* vol. 8, pp. 65-78, 2023.

[35] S. Sorel, “Improved composition to be used as a Cement and as a Plastic Material for Molding Various Articles,” *United States Patent Office. Patent,* vol. 53, no. 092, pp. 6, 1866.

[36] S. A. Walling, and J. L. Provis, “Magnesia-based cements: a journey of 150 years, and cements for the future?,” *Chemical reviews,* vol. 116, no. 7, pp. 4170-4204, 2016.

[37] Y. Zheng, Y. Zhou, X. Huang, and H. Luo, “Effect of raw materials and proportion on mechanical properties of magnesium phosphate cement,” *Journal of Road Engineering,* vol. 2, no. 3, pp. 243-251, 2022.

[38] H. Lahalle, C. C. D. Coumes, C. Mercier, D. Lambertin, C. Cannes, S. Delpech, and S. Gauffinet, “Influence of the w/c ratio on the hydration process of a magnesium phosphate cement and on its retardation by boric acid,” *Cement and Concrete Research,* vol. 109, pp. 159-174, 2018.

[39] B. Xu, B. Lothenbach, A. Leemann, and F. Winnefeld, “Reaction mechanism of magnesium potassium phosphate cement with high magnesium-to-phosphate ratio,” *Cement and Concrete Research,* vol. 108, pp. 140-151, 2018.

[40] G. P. Ganapathy, S. P. Kaliyappan, V. L. Ramamoorthy, S. Shanmugam, A. AlObaid, I. Warad, S. Velusamy, A. Achuthan, H. Sundaram, and M. Vinayagam, “Low alkaline vegetation concrete with silica fume and nano-fly ash composites to improve the planting properties and soil ecology,” *Nanotechnology Reviews,* vol. 13, no. 1, pp. 20230201, 2024.

[41] X. Ren, W. Li, Z. Mao, and M. Deng, “Inhibition of the alkali-carbonate reaction using fly ash and the underlying mechanism,” *Crystals,* vol. 10, no. 6, pp. 484, 2020.

[42] P. Shafigh, S. Yousuf, Z. Ibrahim, B. Alsubari, and I. Asadi, “Influence of fly ash and GGBFS on the pH value of cement mortar in different curing conditions,” *Advances in concrete construction,* vol. 11, no. 5, pp. 419-428, 2021.

[43] L. Sequeira, J. Forero, M. Bravo, L. Evangelista, and J. de Brito, “Durability of concrete with partial replacement of Portland cement by incorporating reactive magnesium oxide and fly ash,” *Materials,* vol. 16, no. 7, pp. 2670, 2023.

[44] R. E. Melchers, *Modelling the long term atmospheric corrosion of aluminium alloys*, Research Report 278.04. 2010, The University of Newcastle, New South Wales …, 2010.

[45] P. Henry, “Diffusion in absorbing media,” *Proceedings of the Royal Society of London. Series A. Mathematical and Physical Sciences,* vol. 171, no. 945, pp. 215-241, 1939.